REVIEW OF SCIENTIFIC INSTRUMENTS **77**, 064903 (2006)

Real-time detection of ambient aerosols using photothermal interferometry: Folded Jamin interferometer

Arthur J. Sedlacek III[a)]
Atmospheric Sciences Division, Environmental Sciences Department, Brookhaven National Laboratory, Upton, New York 11973-5000

(Received 24 January 2006; accepted 25 April 2006; published online 20 June 2006)

Work in our laboratory has been directed at the development of a new class of instrumentation that can directly measure ambient aerosol absorption through photothermal interferometry. The hallmark of this approach is its ability to *directly measure aerosol absorption without interference from aerosol scattering* since the signal originates from the thermal dissipation of the spectrally absorbed energy. While the principle of the photothermal technique for the detection of aerosols was demonstrated in the mid-1980s, this interferometric technique remains a laboratory technique largely due to sensitivity to mechanical vibrations and other environmental factors that result in unwanted signal interference and commensurate reduction in detection sensitivity. In order to realize its application outside the laboratory, a folded Jamin interferometer design has replaced both the traditional Mach-Zehnder and unfolded Jamin configurations. The folded Jamin affords many advantages, which include high degree of common mode noise rejection, insensitivity to rotation and translation of optical components, inherent double pass configuration, and compact size. In this article, we report on the performance of this optical configuration and present representative data for both absorbing and nonabsorbing aerosols. © *2006 American Institute of Physics.*
[DOI: 10.1063/1.2205623]

INTRODUCTION

The contribution of aerosol radiative forcing to the global radiation balance is now recognized as an effect that must be incorporated in our climate models if accurate predictions of climate are to be realized.[1–6] However, the quantitative influence of aerosols on the radiation balance remains one of the most uncertain components of climate change models.[7] More recently, Schwartz[8] has cited that this uncertainty needs to "be reduced by at least threefold for uncertainty in climate sensitivity to be meaningfully reduced and bounded." To achieve this goal, improvements in climate modeling, *in situ* measurements, and fundamental laboratory studies are all required. Specific to the present work is improvement in our understanding of "direct" forcing via aerosol absorption. These forcings can be of a magnitude comparable to those induced by anthropogenically released greenhouse gases, yet, depending upon the degree of aerosol absorption, can be *either* the opposite sign [negative (cooling)] or same sign [positive (warming)].[2,9–11] Hence, it is highly desirable that careful laboratory and field measurements of aerosol optical properties are undertaken so a more rigorous understanding of aerosol climate forcing can be developed.

The most common method for the measurement of aerosol absorption is to measure the change in optical transmission of particulates deposited onto a filter.[12,13] While the filter-based approaches offer several advantages (e.g., commercial availability, unattended operation, robustness, operational inside an aircraft, low-tech method, and relatively fast response time), these filter-based techniques possess significant drawbacks that warrant cautious use. Chief among these drawbacks is artifact absorption. For example, artifact absorption can originate from particulate and/or filter substrate light scattering, as well as multiple absorptions. Both processes can result in an overestimate of the true absorption. Bond *et al.*[12] have reported that all filter-based measurements of aerosol absorption display some response to scattering by particles. Specifically they found that these techniques exhibit a response ranging from 2% to 9%, depending upon the particular technique employed [particle soot absorption photometer (PSAP), integrating plates (IPs), or hybrid integrating plate system (HIPS)]. Interestingly, despite correction for this artifact, absorption measured via these filter methods on reference samples was still found to be too large by 20%–30%. Other potential issues with filter-based approaches are evaporation of semivolatile material from the particle after collection and the potential influence of the substrate on the optical properties of the collected particles themselves. An example of the latter includes absorption values less than zero, as might occur if a hygroscopic particle were to wet the filter material, thereby increasing the transmittance through the filter in a fashion similar to the "wet T-shirt effect." It should be noted that the multiangle absorption photometry (MAAP) approach under development by Schönlinner and co-workers has demonstrated success at overcoming some of the artifactual absorption issues.[14,15]

In an effort to address some of the difficulties associated with the filter-based techniques, a new class of instruments capable of directly measuring aerosol absorption is being

[a)]Electronic mail: sedlacek@bnl.gov

developed: photoacoustic spectroscopy[16] and, the subject of this article, photothermal interferometry (PTI). The hallmark of these approaches is that they *directly measure aerosol absorption without interference from aerosol scattering* since their respective signals originate from the thermal dissipation of spectrally absorbed energy. In the specific case of PTI, aerosol absorption is measured through the refractive index change that accompanies this energy transfer process. In contrast, photoacoustic spectroscopy (PAS) measures the concomitant acoustic shock wave that is generated following light absorption. Despite being originally developed in the early 1980s,[17,18] and even demonstrated for measuring aerosol absorption,[19–21] the photothermal technique has seen limited application.[22–24] This limited use can be traced to the sensitivity of some of these early interferometer designs to mechanical vibrations which required elaborate vibration isolation schemes. However, as will be discussed, the use of a folded Jamin configuration can greatly reduce these noise contributions to negligible (manageable) levels and remove sensitivity of the measurement to optical component rotation and translation.[25–28]

EXPERIMENT

Background. Lin and co-workers[19–21] described the *in situ* measurement of the aerosol absorption of ammonium sulfate using, what the authors referred to as, phase fluctuation optical heterodyne (PFLOH) spectroscopy.[17,18] These initial instruments used a Mach-Zehnder (MZ) configuration, where one arm of the interferometer consisting of a single-frequency laser (He–Ne), initially split by a 50/50 beam splitter (BS), was directed into a sample cell and where and a counterpropagating "pump" laser (line-tunable CO_2) overlapped this "probe" beam.

Absorption of the pump laser light by the aerosol resulted in local heating, which, in turn, caused an expansion of the air in the cell. As discussed above, this expansion results in a change in the refractive index that causes the path length taken by the probe He–Ne beam, relative to the reference arm, to change: in other words, creation of a phase shift, $\Delta\phi(t)$, between the two arms of the interferometer. Upon exiting the cell, the probe beam was directed toward a second BS that recombined the two arms of the interferometer creating the interference pattern that was subsequently detected by a single-element detector. It is this phase shift, which is proportional to the change in index of refraction, Δn, that can be related to the induced temperature increase, ΔT, via the Gladstone-Dale equation,

$$\Delta n = [(n-1)/T_o]\Delta T. \tag{1}$$

Theory. If we let the optical fields of the signal (probe beam) and local oscillator (reference beam) be represented by

$$E_{\text{probe}} = A_{\text{probe}} \cos[\omega_{\text{probe}} + \phi_{\text{probe}} + \Delta\phi(t)],$$
$$E_{\text{ref}} = A_{\text{ref}} \cos(\omega_{\text{ref}} + \phi_{\text{ref}}), \tag{2}$$

where A_j, ω, and ϕ represent the amplitude, angular frequency, and phase; and, where $\Delta\phi(t)$ is the induced time-dependent phase fluctuations introduced above, it can be shown, for a square law detector, that the current in the detector, $I(t)$, is

$$I(t) = \left(\frac{e\eta}{h\nu}\right)\{P_{\text{probe}} + P_{\text{ref}} + 2\sqrt{P_{\text{probe}}P_{\text{ref}}}[\cos(\phi_{\text{probe}} - \phi_{\text{sig}}) - \sin(\phi_{\text{probe}} - \phi_{\text{sig}})\Delta\phi(t)]\}. \tag{3}$$

Here, we have introduced factors that account for detector responsivity, namely, e the electronic charge, η the detector quantum efficiency, and $h\nu$ the laser energy, and have explicitly accounted for the laser power, P_j. In order to realize optimal (read: linear) detection sensitivity, the relative path lengths for the two arms of the interferometer are adjusted so that the system is in quadrature; that is, $\phi_{\text{ref}} - \phi_{\text{probe}} = (2n+1)\pi/2$. Under these conditions, the detector current reduces to

$$I(t) \propto \left(\frac{e\eta}{h\nu}\right) 2P_o \sin\Delta\phi(t) = \left(\frac{e\eta}{h\nu}\right) 2P_o \Delta\phi(t), \tag{4}$$

where we have made the laser power in each arm of the interferometer the same ($P_o = P_{\text{probe}} = P_{\text{ref}}$) and, for small $\Delta\phi(t)$, let $\sin\Delta\phi(t) \approx \Delta\phi(t)$. The value of this expression is that it enables us to formulate an expression for the signal-to-noise ratio (SNR),

$$\text{SNR} = \frac{I_{\text{sig}}^2}{I_{\text{noise}}^2} = \frac{(e\eta/h\nu)^2 P_o^2 \Delta\phi^2}{2e(e\eta/h\nu)P_o\Delta f} = \frac{\eta P_o \Delta\phi^2}{h\nu\Delta f}, \tag{5}$$

where Δf is the signal processing bandwidth, and where we have assumed that shot noise dominates and thus neglected contributions from dark current and Johnson noise. This expression can be rearranged in terms of $\Delta\phi$ to allow estimation of the minimum detectable phase shift,

$$\sqrt{\frac{h\nu\Delta f}{\eta P_o}} = \Delta\phi_{\text{min}}, \tag{6}$$

where SNR has been set to 1. For example, the projected minimum detectable phase shift for a 632.8 nm HeNe operating at 1 mW output power, a detector efficiency of 0.6, and a 1 Hz bandwidth is $\sim 2\times 10^{-8}$ rad. The recent work of Owens *et al.*[22] has realized detection sensitivities within a factor of 4 of this quantum noise limit (*vide infra*).

If we assume that the variation of the refractive index along the path of length l is uniform,[29] the phase shift of the signal will then be given by

$$\Delta\phi = \frac{2\pi l}{\lambda}\frac{(n-1)}{T_o}\frac{\alpha P_{\text{exc}}}{4\pi a^2 \rho C_p f}, \tag{7}$$

where f is the modulation frequency of the excitation beam (e.g., 50 Hz); C_p is the specific heat of air (1005.4 J kg^{-1} K^{-1}); ρ is the density of air (1.205 kg m^{-3}); α is the absorption coefficient of the particle; P_{exc} is the excitation laser power (e.g., 200 mW); λ is the probe/reference wavelength (632.8 nm); a is the radius of the pump beam (e.g., 1 mm); T_o is the absolute temperature (300 K); and n is the index of refraction of air (1.000 292). Combining Eqs. (7) and (6) and solving for α result in an expression enabling an estimate of the minimum detectable absorption coefficient,

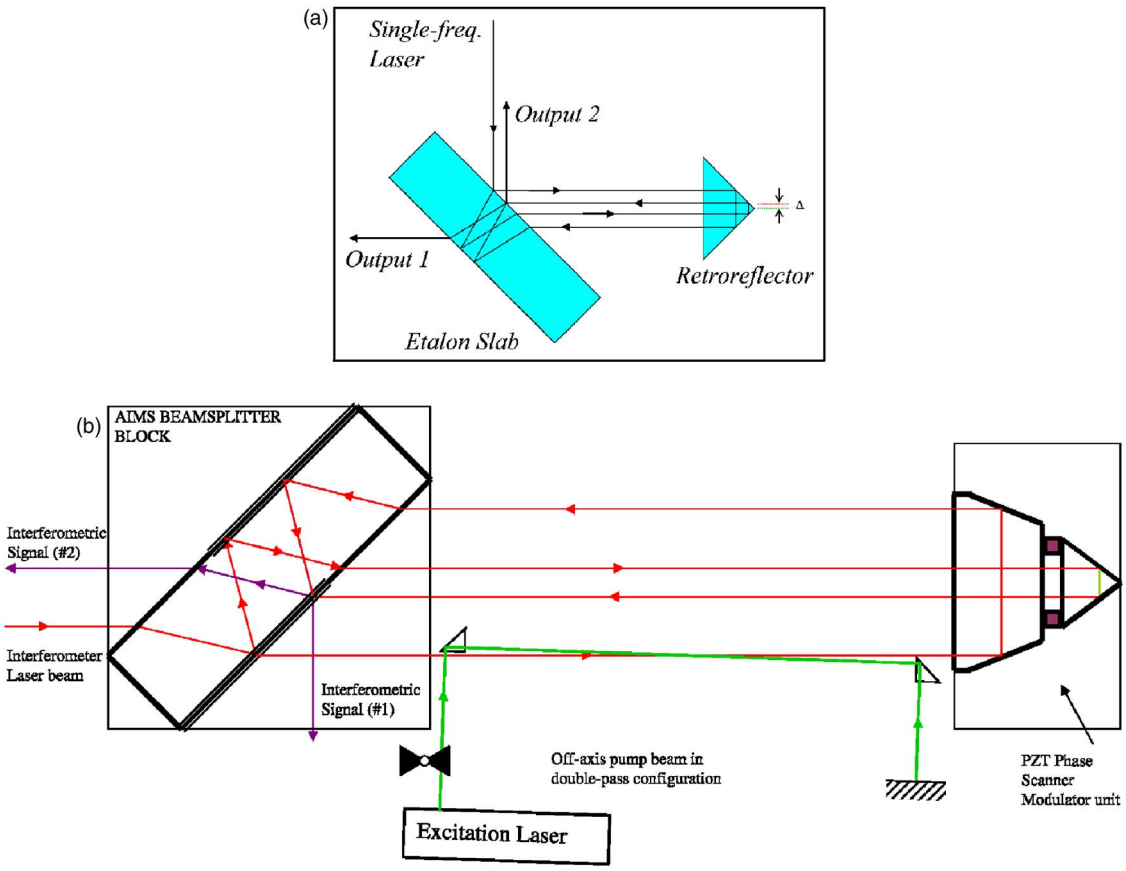

FIG. 1. (Color online) The upper panel depicts a generalized folded Jamin interferometer outfitted with a Porro prism retroreflector (adapted from Ref. 26). Reducing the retroreflector offset from the geometric centerline (i.e., $\Delta \rightarrow 0$) results in a Sagnac interferometer. The lower panel is a schematic of the folded Jamin interferometer built by Interferomet (Ref. 31) and modified for use with the photothermal technique. The red lines trace the single-frequency HeNe laser through the interferometer, while the purple lines represent the interfering signals generated when the two arms of the interferometer are recombined. The green ray traces the pump laser which is arranged in a glancing configuration to eliminate spurious signal generation within shared optics. See text for details. Schematic adapted from Ref. 30.

$$\alpha_{\min} = \frac{2a^2 \rho C_p f \lambda T_o}{(n-1) l P_{\text{exc}}} \sqrt{\frac{2h\nu}{\eta P_o}}. \tag{8}$$

Using the values cited above, a minimum detectable absorption coefficient is estimated to be $\sim 1\ \text{Mm}^{-1}$, a sensitivity level commensurate with that needed to measure expected aerosol absorption levels ($0-100\ \text{Mm}^{-1}$).

Instrument design: Folded Jamin interferometer. A folded Jamin (FJ) interferometer is a variation of a Sagnac interferometer except the paths that the two counterpropagating arms do not overlap. This nonoverlapping configuration can be accomplished by shifting a retroreflector by a small distance relative to the geometric center of the interferometer. Figure 1(a) depicts a generic folded Jamin interferometer. What makes this interferometric design especially appealing is the inherent optical stability of the configuration. As pointed by Moosmüller and Arnott,[26] the folded Jamin configuration allows the realization of a virtually vibration-insensitive interferometer since this configuration is insensitive to rotation and translation of the two optical components that make up the interferometer.

As discussed above, in order to realize maximum sensitivity it is critical to ensure that the interferometer is locked onto the quadrature point. In previous interferometer designs utilizing either the Mach-Zehnder or *unfolded* Jamin configurations, this was accomplished by having one optical component (e.g., mirror or etalon, respectively) outfitted with a piezoelectric transducer (PZT). Directing a portion of the output of the interferometer signal through a feedback circuit, a correction voltage could then be applied to the PZT so that the position of the component can be shifted slightly resulting in a change in the phase between the two interferometer arms thereby enabling the quadrature condition to be maintained. However, the nature of the folded Jamin design effectively precludes this straightforward approach from being used (recall insensitivity to component rotation and translation) thereby requiring more creative methods to obtain quadrature. One approach, suggested by Moosmüller and Arnott,[26] is to exploit polarization. In this approach, a circularly polarized HeNe beam is split into its ***s*** and ***p*** components such that the two counterpropagating arms that make up the folded Jamin configuration are made up of the differing polarizations. In this event, the use of a variable retarder to adjust one polarization enables the system to be brought into quadrature. An alternative approach, and the one taken here, is to split the retroreflector widthwise into two parts and to connect these two halves together through a PZT. This unique configuration is the basis for a recently available folded Jamin interferometer originally developed for high-

precision metrology applications such as measurement of length, angle, vibration, as well as gas and liquid refractivities.[30] Depicted in Fig. 1(b) is a schematic of Interferomet's AIMS folded Jamin interferometer[30] that has been modified for application with the photothermal technique. The two counterpropagating HeNe beams are arranged such that one arm [i.e., outer beam in Fig. 1(b)] intersects with the large retroreflector while the other arm [i.e., inner beam in Fig. 1(b)] reflects off the smaller retroreflector. The main advantage of this approach over the polarization approach is the requirement for fewer optical components.

As the details of the AIMS unit can be found on the manufacturer's website,[30] only the most salient points relevant to the present discussion will be highlighted here. As depicted in Fig. 1(b), a 50/50 beamsplitting coating on the front surface of the etalon slab splits the focused, incoming HeNe laser. The 50% that is reflected from this front surface is subsequently reflected off the totally reflective back surface thereby creating the requisite two arms of the interferometer. Both beams are then directed towards the specially designed retroreflector assembly alluded to above that has been offset slightly from the geometric center axis. In this way, two nonoverlapping sets of beams are generated. Upon reflection off of the retro assembly, the two counterpropagating beams are then recombined at the etalon to generate the interference patterns that are detected by two *p-i-n* diodes. Shifts in the interference pattern can then be monitored through phase sensitive detection techniques.

For the present photothermal application, a pump beam must be overlapped with one arm of the interferometer. While there are a small number of choices available on how to do this, care must be exercised to ensure that unwanted noise is not brought into the system that would compromise overall detection sensitivity. Examples of unwanted noise include pump beam leakage into the "reference" arm, localized heating within those optical elements shared by the HeNe and pump beams due to absorption at the pump wavelength, detection of residual pump beam by *p-i-n* diodes due to light leakage through filters, and nonsymmetric attenuation of the two interferometer beams within the optical train. During the course of testing, two optical configurations were tried: (i) a polarizing beamsplitter cube and (ii) a glancing angle configuration [as depicted in Fig. 1(b)]. In the former configuration, a polarizing beamsplitter cube (CVI Laser Corp.) was used to overlap the pump beam with one arm of the interferometer. Specifically, the polarizing cube, centered on the inner beam path passes the ***p***-polarized HeNe beam while reflecting the ***s***-polarized pump wavelength. The advantage of this optical arrangement is that it enables complete overlap between the sample arm and the pump beam. However, under high-sensitivity conditions it was observed that the base line is not stable due to localized heating within the polarizing cube. For example, typical signal levels for the 15 mW 532 pump laser (Brimrose) chopped at 100 Hz was 20 μV, whereas the typical base line without 532 beam was 250 nV. Clearly this two order-of-magnitude increase in base line is unacceptable. Consequently an alternate optical configuration was considered: a glancing arrangement where the pump beam was brought in at a 1°–2° angle relative to the HeNe beam using a 3 mm folding prism. Employment of an off-axis alignment has been successfully used in the past by Owens *et al.*[22] and Mazzoni and Davis.[29] While this configuration does sacrifice interaction path length, it completely eliminates many of the interference effects attributable to localized heating within shared optical components. The use of a mirror after the second folding prism enables a double pass of the pump beam further minimizing signal loss with this configuration, as shown in Fig. 1(b).[29]

In an effort to eliminate thermal gradients across the beam paths originating from the laser power supplies and/or draughts, a Lexan-based enclosure was constructed that housed only folding optics and sample cell. In addition to this, the inside of the Lexan enclosure was lined with an acoustic isolation material (Hushcloth). At a 1 in. thickness, this material provides a 0.9 absorption coefficient from 1000 to 4000 Hz and nominally 0.75 from 500 to 1000 Hz. As an added measure to the Hushcloth, the outside of the enclosure was lined with Whispermat™. This results in a three-layered enclosure (Whispermat-Lexan-Hushcloth) enabling data acquisition in noisy environments (e.g., laboratory hood fans, and talking, running pumps) without compromising detection sensitivity.

Measurement details. The interference patterns measured by the *p-i-n* diodes (Centronic OSD 5-5TB Si photodiode outfitted with "bugs-eye lens") were monitored using phase sensitive detection employing a Stanford Research System lock-in amplifier (SRS-850). The reference frequency is provided by the "trigger out" from the mechanical chopper (SRS-540). The LIA was interfaced to a laptop computer (Dell, Latitude 840C) via USB-GPIB (National Instruments) for data acquisition, storage, and subsequent analysis. Typical detection bandwidths were 26 mHz (3 s time constant), 7.8 mHz (10 s time constant), or 2.6 mHz (30 s time constant).

The interferometer laser was a single-frequency HeNe from Melles Griot (05-STP series). A 3 min wedge was incorporated into the HeNe optical train before entry into the Jamin head to prevent back reflections to the laser head. The 514 nm (and 248 nm) pump laser (Coherent argon ion laser model 300c FreD with the capability of intracavity doubling) had an adjustable power from 100 mW to 1.5 W (2–30 mW at 248 nm) that was measured using a power meter (Newport model 818-UV and Ophir model 30A). Following a warm-up period (~30 min) the interferometer alignment was optimized by monitoring the Lissajous circle generated when the two 90° out of phase outputs from the *p-i-n* diodes were fed into an oscilloscope (LeCroy 9350AM). Once optimized, the output from one of the *p-i-n* diodes was connected to a servo-control feedback circuit designed to lock onto quadrature.[30] This circuit maintains quadrature by applying a correction voltage to the PZT connecting the two halves of the retro assembly. This circuit applies a correction voltage to the PZT for slow unmodulated temperature drifts in the system while completely ignoring the transient temperature changes induced by the modulated pump laser. Figure 2 shows PTI signal as a function of modulation period for a 1 μl sample of acetone in a 5 cm sample cell. For these measurements, the pump laser is tuned to 248 nm to access

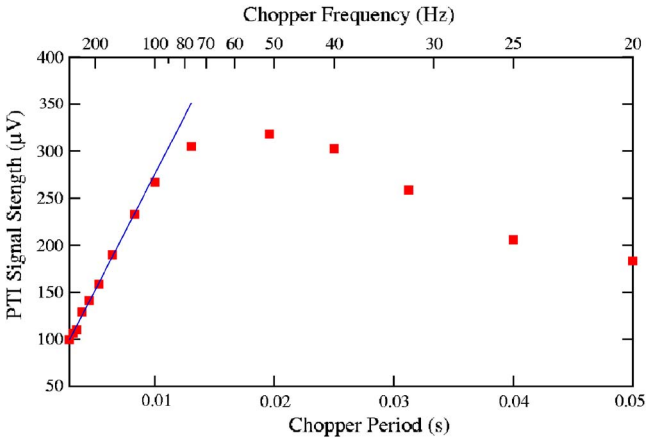

FIG. 2. (Color online) PTI signal as a function of modulation period. The PZT servo feedback circuit is designed to correct for slowly varying thermal drifts that occur on the order to 1–10 s. These data show that the optimal modulation frequency is on the order 100 Hz. The blue line depicts the $1/f$ dependence of the PTI signal at high chopping frequencies.

the acetone $n \rightarrow \pi^*$ transition.[31] From the figure it is easily seen that the optimal modulation frequency is about 100 Hz. As a result, all measurements are conducted at ~100 Hz to avoid any unnecessary signal attenuation. Prior to entering the cell, the pump beam is focused by an $f/6$ lens so that the beam waist overlaps the HeNe beam in the center of the sample cell. Finally, the spatial resolution of this folded Jamin interferometer, with servo feedback to maintain quadrature, is subpicometers (e.g., for a 1 V peak-to-peak Lissajous figure a 1 nm path length change will generate a 10 mV signal, *vide infra*).

Nitrogen dioxide at 11 ppm was procured from Scott Gases (Certified Working Class) while nitrogen was obtained in house (minimum purity of 99.9%). The gases were metered into the sample cell using a Tylan four-channel flow controller (model RO-28) outfitted with a 1 l/min and 0.1 l/min mass flow controller (model FC-280). Acetone was spectroscopic grade (Mallinckrodt) and aliquots were provided by a micropipette (Chempette, Series 7947) in quantities ranging from ~100 nl to 5 μl. The 5 cm path length sample cell was UV-grade quartz (NSG Precision Cell, type 35) and had a volume of 75 cm^3. For those experiments involving aerosols, two types were used: black carbon (BC) which represents an absorbing aerosol and the nonabsorbing (at 514 nm) ammonium sulfate. The glassy carbon was obtained from Aldrich (99.95%). For the BC experiments, a small amount of the material was placed at the bottom of an impinger whereupon nitrogen, flowing at 1 l/min, was turned on for 30 s and then turned off. This action resulted in a "puff" of BC into the sample cell. The nominal particle density into the cell was on the order of 5000 particles/cm^3 as measured with TSI's condensation particle counter (model 3025). Once the air stream was cleared of BC, a 0.1 l/min flow of NO_2 was released into the cell to verify operation of the instrumentation. In contrast, the $(NH_4)_2SO_4$ was generated using a constant output atomizer (TSI model 3076). For the proof-of-principle experiments conducted here, a 0.125% solution of ammonium sulfate was used. Again, as with the BC experiments, once the air stream was cleared of the aerosol, a 0.1 l/min flow of NO_2 was released into the cell. The particle count for the ammonium sulfate exceeded the dynamic range of the CNC (10^5 cc^{-1}) and is estimated to be 10^7 particle/cm^3 based on the TSI constant output atomizer user manual and performance specifications.

RESULTS AND DISCUSSION

The first set of experiments carried out at 514 nm involved performance measurements using a calibrated quantity of nitrogen dioxide. When conducting a pump-and-probe-type experiment involving phase sensitive detection it is imperative that great care be taken to eliminate stray pump light leakage into the field of view of the detectors that monitor the interference pattern. In the case of the 514 nm pump, the required high rejection ratio of pump beam to interferometer beam was made slightly complicated by the close proximity of this wavelength to the interferometer wavelength at 632 nm. However, by using a combination of a long-pass filter and narrow-bandpass filter centered at the HeNe wavelength the high rejection ratio necessary was achieved. Specifically, the 2 in. square long-pass filter (OG-570, >90% transmission at 632 nm and O.D. 4 at 514 nm) covered both the HeNe exit and return ports on the Jamin head while the $\frac{1}{2}$ in. bandpass filters (CVI Laser; 90% transmission at 632 nm and O.D.>5 off central wavelength) were placed in front of the return ports only since the *p-i-n* diodes are aligned to these ports. This arrangement also ensured that there was symmetric attenuation of both interferometer arms.

Experiments measuring the PTI signal as a function of laser power resulted in the expected linearity [cf. Eq. (7)], with a correlation coefficient exceeding 0.999 for a detection bandwidth of 7.8 mHz and a modulation frequency of 94 Hz. For these experiments the laser power was taken as the average value measured for the duration of a given laser power setting. The added utility of this measurement is that it provides information regarding minimum laser power requirements for signal extraction for in-field deployment. This set of experiments was then followed by the examination of the PTI signal linearity to the analyte concentration. A representative example of the raw signal as a function of concentration in a time series is shown in the upper panel of Fig. 3 while the lower panel contains the plot of the PTI signal versus NO_2 concentration [in parts per billion (ppb)] from several independent experiments. The slope of the lower trace can be used to calculate the NO_2 absorption coefficient at 514 nm and is found to be $2.2 \pm 0.08 \times 10^{-19}$ cm^2/molecule. This value compares favorably with the average of $1.8 \pm 0.2 \times 10^{-19}$ cm^2/molecule that was estimated from the work of Davidson *et al.*,[32] Vandaele *et al.*,[33] Vandaele *et al.*,[34] Harder *et al.*,[35] Voigt *et al.*,[36] Schneider *et al.*,[37] Harwood and Jones,[38] and Burrow *et al.*[39] Converting the NO_2 concentration from ppb to absorption coefficient (Mm^{-1}) and extrapolating to the LIA base line of 300 nV (rms value of the base line absent any NO_2) a detection sensitivity approaching ~200 Gm^{-1} is predicted (or about 0.3 ppb). This extrapolation is within a factor of 7 of that

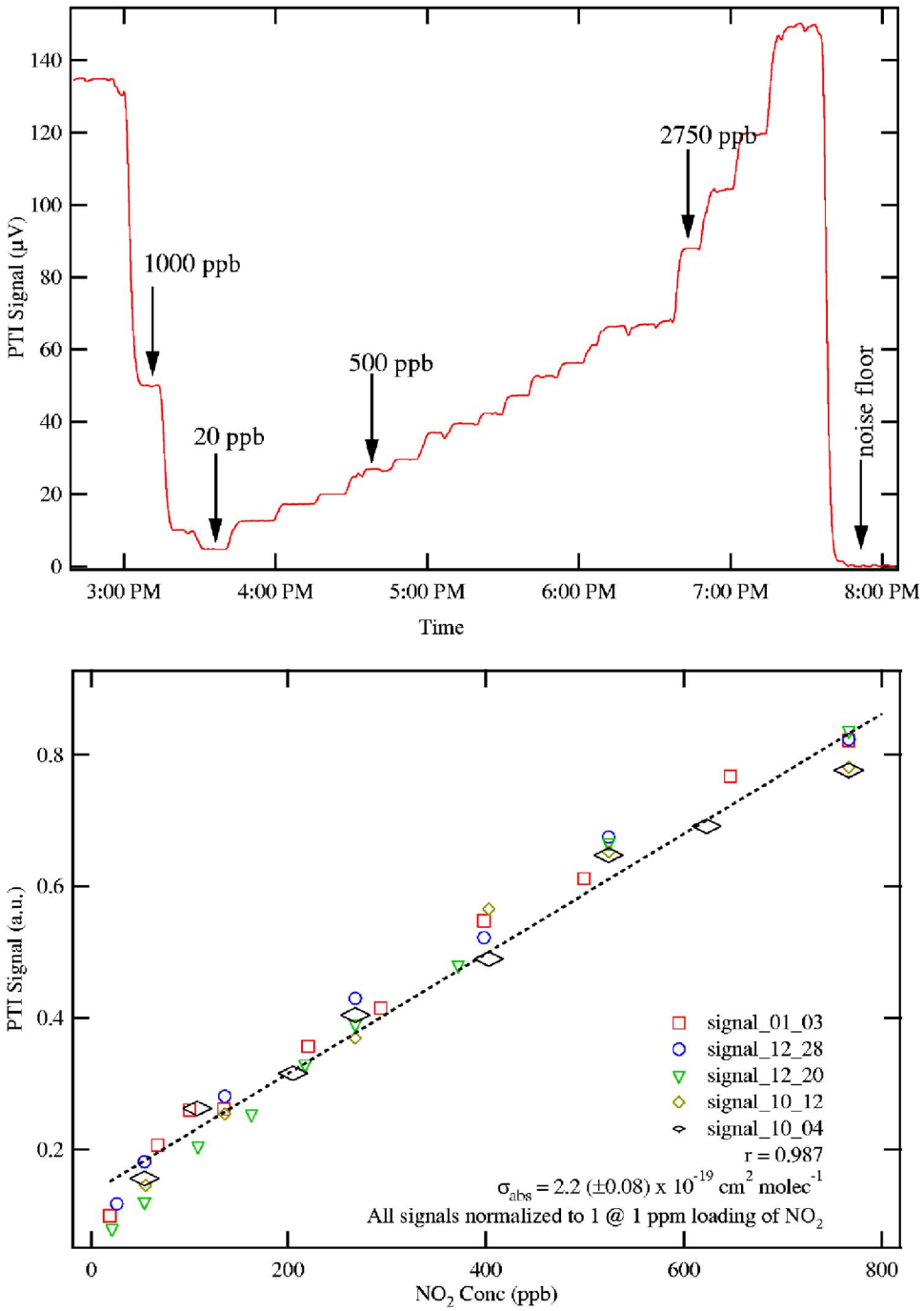

FIG. 3. (Color online) PTI signals for NO_2. Top trace shows an example of the PTI signal for a time series of NO_2 loadings in the sample cell while the lower trace is a plot of independent measurements of the PTI signal vs NO_2 concentration. Numbers cite in upper trace is the NO_2 loading in ppb. The calculated absorption coefficient is based on best fit. See text for details.

predicted using Eq. (8). In 1982, Campillo *et al.*[40] used a stabilized Fabry-Pérot cavity to measure NO_2 and cited an extrapolated detection limit of 7 ppb with a 3 W, 514 nm excitation source or about 3.5 Mm^{-1}. As an additional reference point on the projected detection sensitivity, Owen *et al.*[22] reported a sensitivity of 37 Gm^{-1} for ammonia at 1085 cm^{-1} using an unfolded, 38 cm path length Jamin interferometer. It should be noted that the absorption cross section for the sR(5, 0-5) rotational states of ammonia at 1084.6 cm^{-1} is $3.6\times10^{-18}cm^2$/molecule or about 10× larger than the absorption cross section for NO_2 at 514 nm.[41] Obvious improvements, discussed in further detail below, such as increasing the path length from 5 to 25 cm would increase the detection sensitivity to 40 Gm^{-1}. The departure from linearity observed at higher concentrations indicates the onset of effects attributable to thermal lensing caused by large temperature gradients present under the higher NO_2 loading levels. However, using the current configuration, the linear region does span four orders of magnitude and can be extended to higher concentrations by decreasing the pump laser intensity or increasing the chopping frequency. Since the photothermal technique is based on the dissipation of heat, data from readily available molecular standards such as NO_2 can serve as the calibration standard for the measurement of absorption of aerosols.

Figures 4 and 5 show PTI signals obtained from BC and ammonium sulfate (nonabsorbing aerosol at 514 nm), respectively. The nominal BC particle density of 5000 particles/cm^3 as measured with TSI's condensation particle counter. Once the BC was cleared out of the sample

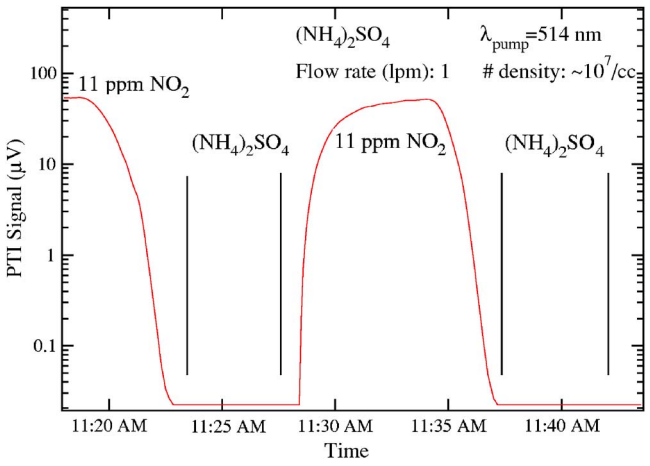

FIG. 4. (Color online) PTI signals for "puff" of black carbon. Signal for 11 ppm of NO_2 demonstrates that the unit is operating correctly.

chamber (as evidenced by a commensurate decrease in the PTI signal), a 0.1 l/min flow of NO_2 was released into the cell to verify operation of the instrumentation. This was again followed by another 30 s puff of BC. The presence of BC at this particle density is clearly discernable against the base line. The detection bandwidth for these measurements was 7.8 mHz and the nominal laser power was 250 mW. It should be noted that the differing rise times between the black carbon and the NO_2 reflect the differing flow rates used in the two channels: 1 l/min for the aerosol channel and 0.1 l/min for the NO_2. In contrast to the BC signals, when a pure aerosol scatterer is injected into the flow cell no signal is observed, as expected. This is exemplified by the interrogation of a 10^7 particle/cm^3 density of ammonium sulfate. Despite loading the sample cell with a particle density that was nearly four orders of magnitude higher then that used in the BC experiments, the complete absence of an absorption channel results in no PTI signal. Following the injection of the ammonium sulfate, NO_2 is again introduced into the cell, in an analogous fashion as that done with BC, to confirm the

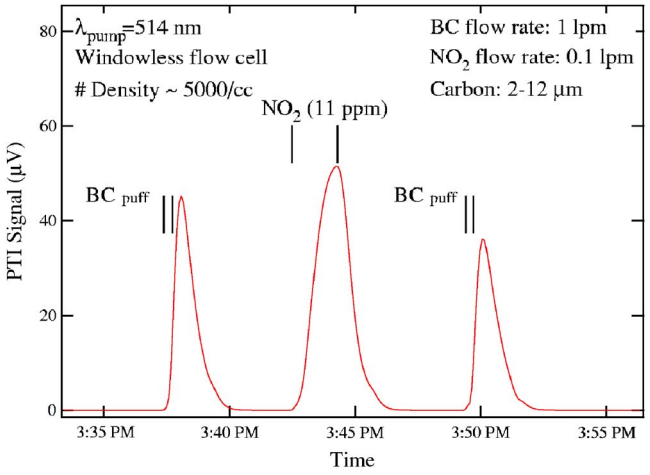

FIG. 5. (Color online) Ammonium sulfate does not absorb at 514 nm, thus there should be no photothermal signal. These data also demonstrate that PTI suffers no interference from light scattering.

instrument is within nominal operational parameters. Data acquisition parameters are the same as that used for the BC experiments.

With the conclusion of these proof-of-principle experiments, it is instructive to conduct a top-level evaluation of areas where the performance of this instrument could be further improved. One high priority improvement would be to incorporate a multispectral capability. Such a capability would increase the utility of the instrument by either allowing multiple species to be studied simultaneously and/or for increased finesse of a single species measurement by enabling simultaneous measurement at multiple "on" and "off" absorption wavelengths. One obvious approach to realize this capability would be to copropagate into the sample cell several pump wavelengths of interest where each is modulated at a unique frequency that is not an integer of another modulation frequency. The resultant data set could then be demodulated using either multiple lock-in amplifiers or by taking the Fourier transformation from temporal space to frequency space. This approach can be extended to any number of pump wavelengths.

Another obvious improvement would be to incorporate a higher power pump laser for increased detection sensitivity, along with the already cited increase in path length. A less obvious but just as potentially valuable improvement would be to replace the single-frequency HeNe laser with a single-frequency blue laser. Since the sensitivity of the PTI approach goes as the square root of the interferometer wavelength and inversely as the power of that laser [cf. Eq. (8)] replacement of the 1 mW HeNe with a 5 mW 430 diode pumped solid-state (DPSS) laser (e.g., Melles Griot 85-BTL-005-115) would be expected to increase the detection sensitivity by nominally 6× (with all other things being kept constant). However, issues associated with a larger linewidth and phase noise relative to the HeNe laser could limit the overall sensitivity increase via this approach. Top-level examinations of potential improvements such as these outlined here ultimately provide information that can be readily utilized in instrument design flexibility. For example, the performance enhancement that could be realized by incorporating the blue laser discussed above would allow the sample path length to be decreased while still maintaining a given detection sensitivity. Such a decrease in path length would result in a more robust platform.

Finally, the current interferometer design still possesses moving parts that could potentially translate into unwanted noise. While the polarization-based folded Jamin design suggested by Moosmüller and Arnott[26] possessed no moving parts it was felt that the increased complexity of this design offset the benefits. However, there is a slight modification to the present interferometer configuration that would result in a design that had no moving parts: replacement of the nontunable interferometer laser (HeNe) with a single-mode, continuously tunable diode laser. Incorporation of a tunable laser would allow the use of a single solid retroassembly since quadrature could then be obtained by simply tuning the frequency of the laser (via the injection current into the semiconductor laser) as opposed to using a PZT actuator. Recall that emission wavelength of a diode laser is controlled by the

variation of the injection current and/or temperature.[42] The obvious advantage of this is that the entire unit would not possess any moving parts with no additional optical components thereby resulting in a unit with very high degree of mechanical stability. Interferometry utilizing tunable lasers has been employed for surface profilometry[43] and length metrology.[44] It is interesting to note that Ishii *et al.*[45] suggested that interferometers using phase shifters such as a PZT could be replaced with tunable laser sources.

We have demonstrated that a folded Jamin interferometer can be used to measure photothermal signals generated by either gases or aerosols. The hallmark of the photothermal interferometric technique is that it has very high sensitivity, while the hallmark for the folded Jamin design is superior mechanical stability relative to other interferometer configurations (MZ and unfolded (Jamin). Finally, it was shown that PTI can be used to measure the absorption of aerosols and that aerosol scattering has no effect on the PTI signal.

ACKNOWLEDGMENTS

The author would like to gratefully acknowledge Istvan Dioszegi for his assistance during the onset of this project and Dr. Mike Downs (Interferomet, Ltd.) for the many insightful discussions and electronic mails. This study was supported by the Atmospheric Science Program within the Climate Change Research Division, U.S. Department of Energy under Contract No. DE-AC02-98CH10886.

[1] R. J. Charlson, J. Langner, H. Rodhe, C. B. Leovy, and S. G. Warren, Tellus **43AB**, 152 (1991).
[2] R. J. Charlson, S. E. Schwartz, J. M. Hales, R. D. Cess, J. A. Coakley, J. E. Hansen, and D. J. Hofmann, Science **255**, 423 (1992).
[3] Y. J. Kaufman, D. Tanré, B. N. Holben, S. Mattoo, L. A. Remer, T. F. Eck, J. Vaughan, and B. Chetenet, J. Atmos. Sci. **59**, 635 (2002).
[4] V. Vinoj, S. S. Babu, S. K. Satheesh, K. K. Moorthy, and Y. J. Kaufman, J. Geophys. Res. **109**, D05203 (2004).
[5] J. E. Hansen, J. Sato, and R. Redy, J. Geophys. Res. **102**, 6831 (1997).
[6] J. E. Hansen, J. Sato, A. Lacis, R. Ruedy, I. Tegen, and E. Matthews, Proc. Natl. Acad. Sci. U.S.A. **95**, 12753 (1998).
[7] *Climate Change 2001: The Scientific Basis*, edited by J. T. Houghton, Y. Ding, D. J. Griggs, M. Noguer, P. J. van der Linden, X. Dia, K. Maskell, and C. A. Johnson (Cambridge University Press, Cambridge, 2001), pp. 944.
[8] S. E. Schwartz, J. Air Waste Manage. Assoc. **54**, 1351 (2004).
[9] P. Chylek and J. Wong, Geophys. Res. Lett. **22**, 929 (1995).
[10] J. M. Haywood and K. P. Shine, Geophys. Res. Lett. **22**, 603 (1995).
[11] J. M. Haywood, V. Ramaswamy, and B. J. Soden, Science **283**, 1299 (1999).
[12] T. C. Bond, T. L. Anderson, and D. Campbell, Aerosol Sci. Technol. **30**, 582 (1999).
[13] D. Campbell, S. Copeland, and T. Cahill, Aerosol Sci. Technol. **22**, 287 (1995).
[14] A. Petzold and M. Schönlinner, J. Aerosol Sci. **35**, 421 (2004).
[15] A. Petzold, H. Kramer, and M. Schönlinner, Environ. Sci. Pollut. Res. **4**, 78 (2002).
[16] W. P. Arnott, K. Hamasha, H. Moosmueller, P. J. Sheridan, and J. A. Ogren, Aerosol Sci. Technol. **39**, 17 (2005).
[17] C. C. Davis, Appl. Phys. Lett. **36**, 515 (1980).
[18] C. C. Davis and S. J. Petuchowski, Appl. Opt. **20**, 2539 (1981).
[19] H.-B. Lin and A. J. Campillo, Appl. Opt. **24**, 422 (1985).
[20] D. U. Fluckiger, H.-B. Lin, and W. H. Marlow, Appl. Opt. **24**, 1668 (1985).
[21] A. J. Campillo and H.-B. Lin, U. S. Patent No. 4,415,265 (November 1983).
[22] M. A. Owens, C. C. Davis, and R. R. Dickerson, Anal. Chem. **71**, 1391 (1999).
[23] S. E. Bialkowski, *Chemical Analysis: A Series of Monographs on Analytical Chemistry and its Application*, Photothermal Spectroscopy Methods for Chemical Analysis, Vol. 134 (Wiley, New York, 1996), and all references therein.
[24] N. J. Dovichi, Rev. Sci. Instrum. **61**, 3653 (1990).
[25] S. Namba, Rev. Sci. Instrum. **30**, 642 (1959).
[26] H. Moosmüller and W. P. Arnott, Opt. Lett. **21**, 438 (1996).
[27] H. Moosmüller, W. P. Arnott, and C. F. Roger, J. Air Waste Manage. Assoc. **47**, 157 (1997).
[28] K. P. Birch, M. D. Downs, and R. E. Ward, J. Phys. E **21**, 692 (1988).
[29] D. L. Mazzoni and C. C. Davis, Appl. Opt. **30**, 756 (1991).
[30] Interferomet Inc. West Suxxex, United Kingdom, http://www.interferomet.com.
[31] J. M. Dudik, R. J. Craig, and S. A. Asher, J. Phys. Chem. **89**, 3805 (1985).
[32] J. A. Davidson, C. A. Cantrell, A. H. McDaniel, R. E. Shetter, S. Madronich, and J. G. Calvert, J. Geophys. Res. **93**, 7105 (1988).
[33] A. C. Vandaele *et al.*, J. Quant. Spectrosc. Radiat. Transf. **59**, 171 (1998).
[34] A. C. Vandaele, A. C. Hermans, P. C. Simon, M. Van Roozendael, J. M. Guilmot, M. Carleer, and R. Colin, J. Atmos. Chem. **25**, 289 (1996).
[35] J. W. Harder, J. W. Brault, P. V. Johnston, and G. H. Mount, J. Geophys. Res. **102**, 3861 (1997).
[36] S. Voigt, J. Orphal, and J. P. Burrows, J. Photochem. Photobiol., A 149, 1 (2002).
[37] W. Schneider, G. K. Moortgat, G. S. Tyndall, and J. P. Burrows, J. Photochem. Photobiol., A **40**, 195 (1987).
[38] M. H. Harwood and R. L. Jones, J. Geophys. Res. **99**, 22955 (1994).
[39] J. P. Burrows, A. Dehn, B. Deters, S. Himmelmann, A. Richter, S. Voigt, and J. Orphal, J. Quant. Spectrosc. Radiat. Transf. **60**, 1025 (1998).
[40] A. J. Campillo, S. J. Petuchowski, C. C. Davis, and H.-B. Lin, Appl. Phys. Lett. **41**, 327 (1982).
[41] E. D. Hinkley, R. T. Ku, and P. L. Kelly, in *Topics in Applied Physics*, edited by E. D. Hinkley (Springer-Verlag, New York, 1976), Vol. 14, p. 237.
[42] J. Struckmeier, A. Euteneuer, B. Smarsly, M. Breede, M. Born, M. Hofmann, L. Hildebrand, and J. Sacher, Opt. Lett. **24**, 1573 (1999).
[43] A. Abou-Zeid and P. Wiese, Meas. Sci. Technol. **9**, 1105 (1998).
[44] J. A. Stone, A. Stejskal, and L. Howard, Cal. Lab. Mag. 1–7 (1999).
[45] Y. Ishii, J. Chen, and K. Murata, Opt. Lett. **12**, 233 (1987).